

RESEARCH ARTICLE

Path Loss Model Based on Machine Learning Using Multi-Dimensional Gaussian Process Regression

KI JOUNG JANG¹, SEJUN PARK¹, JUNSEOK KIM², (Member, IEEE), YOUNGKEUN YOON²,
CHUNG-SUP KIM², YOUNG-JUN CHONG², AND GANGUK HWANG¹, (Member, IEEE)

¹Department of Mathematical Sciences, Korea Advanced Institute of Science and Technology, Daejeon 34141, South Korea

²Radio Resource Research Section, Radio and Satellite Research Division, Electronics and Telecommunications Research Institute, Daejeon 34129, South Korea

Corresponding author: Ganguk Hwang (guhwang@kaist.edu)

This work was supported in part by the Institute for Information and Communications Technology Planning and Evaluation (IITP) through the Korea Government (Ministry of Science and Information & Communications Technology, MSIT) under Grant 2017-0-00066 (Development of time-space based spectrum engineering technologies for the preemptive using of frequency), and in part by the National Research Foundation of Korea (NRF) through the Korea Government (Ministry of Science and Information & Communications Technology, MSIT) under Grant NRF-2019R1A5A1028324.

ABSTRACT For beyond fifth-generation (5G) and future wireless communications, spatial consistency that represents the correlation between propagation channel characteristics in close proximity has become one of the major issues in channel modeling to describe channels more realistically in emerging scenarios such as device-to-device (D2D). In this paper, we propose a novel path loss model based on multi-dimensional Gaussian process regression (GPR) that gives spatial consistency to channels in propagation environment by predicting local shadow fading while fitting large-scale path loss from measured data. The proposed model has a special structure consisting of a radial mean function and a local shadow fading term. In contrast to the log-distance path loss model and other regression-based approaches, the special structure of the proposed model provides good spatial consistency. Moreover, since the proposed model is based on GPR, it provides the uncertainty of the predicted path loss. We validate the performance of the proposed model in terms of prediction accuracy with the measurement datasets from two different indoor environments. Our experiments show that the proposed model predicts better than the log-distance path loss model, especially when spatial correlation gets more significant. The proposed model can be also used to simulate path loss in a general environment after training the measurement data.

INDEX TERMS Path loss, multi-dimensional Gaussian process regression, machine learning.

I. INTRODUCTION

Propagation channel model, which characterizes the propagation of radio waves with several channel parameters, is necessary for the design and development of wireless communication systems [1]. Channel parameters such as path loss, propagation delay, Doppler frequency shift, arrival direction and departure direction of each multipath are obtained from the channel impulse response (CIR) measured by a channel sounder or simulated by ray-tracing principles [2], [3]. The propagation channel measurements

using a channel sounder are exploited to develop various stochastic channel models such as non-geometrical stochastic channel models, geometry-based stochastic channel models (GSCMs), and hybrid GSCMs. While the propagation channel is realized using channel parameters that do not reflect the geometry of the propagation environment in the non-geometrical stochastic channel models, e.g. Turin [4], Saleh-Valenzuela [5], GSCMs consider the placement of scatterers for channel realization and include the well-known standard models such as COST 2100 [6], Third-Generation Partnership Project (3GPP) spatial channel model [7], and Winner and Winner II [8]. Clusters that have similar multipath characteristics are modeled in GSCMs and

The associate editor coordinating the review of this manuscript and approving it for publication was Jesus Felez¹.

the inter-cluster and intra-cluster parameters are developed. In hybrid GSCMs, the inter-cluster and intra-cluster characteristics are determined geometrically and stochastically, respectively [9], [10], [11]. The propagation channel simulation using an environment map and ray-tracing principles are exploited to develop map-based models where the propagation channels are realized deterministically [12], [13], [14].

Among the channel parameters, path loss is the most fundamental characteristic of a propagation channel that describes the power attenuation of a signal between transmitter (Tx) and receiver (Rx). Accurate modeling of path loss is vital for system deployment as it determines the received power of a wanted signal and interference powers of unwanted signals in wireless communication systems, which are required for wireless coverage assessment and interference analysis [15], [16], [17].

Statistical path loss models in representative environments, e.g., outdoor urban-macro, urban-micro, rural, and indoor, have been respectively established by various research groups [8], [18], [19], [20], [21], [22], [23] and standardized in 3GPP and International Telecommunication Union (ITU) [7], [24]. The two most widely-used statistical path loss models are the floating-intercept (FI) model and the close-in (CI) model [25], [26]. For the construction of the models, path loss is commonly fitted as the one-dimensional (1D) affine function of a log-scaled distance between Tx and Rx, and the residue from the fitted line is further modeled as a shadow fading. However, these traditional log-distance path loss models cannot fully reflect the propagation environment due to its 1D structure. For example, path losses at different receiving points with the same distance from a fixed TX are considered to be the same in the fitted line and the shadow fading of the receiving points in close proximity are considered as independent [27].

For beyond fifth-generation (5G) and future wireless communications, temporal or spatial evolution of a channel is essential in channel model to fully exploit all the channel states of multi-users connected to a base station (BS) and to evaluate beam-tracking performance along the user equipment (UE) movements [28], [29]. The evolution of a channel should be spatially consistent, which means that channel characteristics between locations in close proximity are highly correlated. Furthermore, not only the scenario that a fixed BS serves multi-users, but also scenarios with both moving link ends such as device-to-device (D2D) and vehicle-to-vehicle (V2V) have to be spatially consistent, i.e., channels between arbitrary locations of Tx and Rx in the environment are all correlated.

There have been various studies to simulate spatially consistent path loss in the environment. In GSCMs, correlation between distinct Rx locations is defined as an exponential function of a distance between the locations and shadow fading is realized by using two-dimensional (2D) exponential filter [7], [30], [31]. However, the models simply consider generating path loss data to vary smoothly in space, not actually predicting the local propagation nature from its nearby

multi-dimensional structure. Moreover, spatial consistency between links with distinct Tx and Rx locations cannot be realized. In map-based models, the propagation status of the environment is described using the ray-tracing principles to reflect the environment [12], [13], [14]. However, the models require precise three-dimensional (3D) geometric description of environment including the constituting materials and their optical propagation properties. Even though it generates the propagation data actually consistent to its environment, it is not practical to apply it for arbitrary environments due to its massive complexity of the required environment description data. Moreover, it is hard to accurately model propagation effects such as diffuse scattering using the ray tracing algorithms.

Giving spatial consistency to path loss is basically a prediction problem at arbitrary locations of Tx and Rx, and this kind of prediction problem can be solved by existing machine-learning methods with the aid of big data and improved computing capabilities [32], [33]. There are also approaches [34], [35], [36], [37], [38], [39], [40] for path loss prediction using various machine learning methods. However, it is difficult to apply them to an arbitrary wireless environment because they need some extra datasets other than path loss such as maps of the environments or focus on one-dimensional fitting between the distance and the path loss, which usually fails to provide good spatial consistency. In [40], the power delay profile (PDP) is used as an input of a neural network to predict channel model parameters. However, to predict path loss at an arbitrary location it needs the PDPs at the location which is unavailable because the PDPs can be obtained only by measurement.

To overcome the limit of the existing methods mentioned above, we propose a new path loss model based on multi-dimensional Gaussian process regression (GPR) that provides path loss predictions at arbitrary link locations in the environment. Compared with other machine learning algorithms, GPR is more appropriate when we develop a predictive model for path loss because it can provide not only predicted values but also their prediction intervals. If we can provide prediction intervals in path loss prediction, we can provide more reliable wireless communication by considering the prediction intervals. This is one main reason why we use GPR in this work. In addition, by gradient descent algorithm GPR automatically finds the optimal parameters to improve efficiency and accuracy of the prediction. The proposed GPR-based path loss model has a special structure consisting of a radial mean function and a local shadow fading term, which is shown to provide good spatial consistency from our experiments. Note that the proposed GPR-based path loss model does not need extra datasets other than path loss.

For validation purpose, we compare the proposed GPR-based path loss model with the log-distance path loss model and the KNN regression model (that is recommended in [41] for path loss prediction) by using the path loss datasets obtained from the measurement campaign in two real indoor

environments. In terms of the prediction error, we see from our experiments that the proposed GPR-based path loss model outperforms the log-distance path loss model and the KNN regression model.

The remainder of this paper is organized as follows: In Section II, we summarize the log-distance path loss model and its drawbacks. In Section III, we explain the KNN regression model and propose our novel path loss model based on the multi-dimensional GPR. In Section IV, we discuss the measurement campaign used in our experiments. In Section V, we provide the experimental details, compare the prediction performance of the models, and discuss our observations. Our conclusions are provided in Section VI. The basic mathematical background on multi-dimensional GPR is summarized in the Appendix.

II. THE LOG-DISTANCE PATH LOSS MODEL

In a log-distance path loss model [42], path loss is considered as the function of a log-scaled distance between the Tx and Rx, i.e.,

$$PL = PL_0 + 10\gamma \log_{10} \frac{d}{d_0} + \chi_\sigma, \quad (1)$$

where PL is the path loss on a dB scale, γ is the path loss exponent, d_0 is the reference distance, d is the distance between Tx and Rx, and PL_0 is the path loss at the reference distance d_0 on a dB scale. Shadow fading is expressed by χ_σ , which follows a Gaussian distribution with mean zero and standard deviation σ . We can simplify the model as

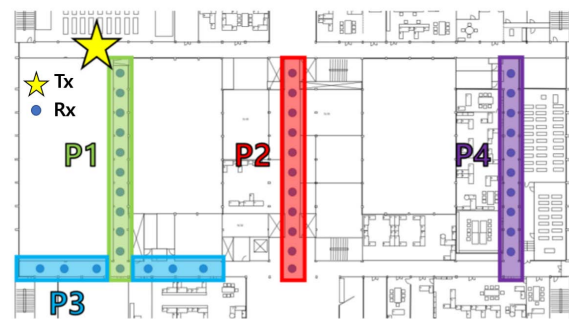
$$PL(d) = \beta_0 + \beta_1 \log_{10} d + \chi_\sigma \quad (2)$$

where $\beta_0 = PL_0 - 10\gamma \log_{10} d_0$ and $\beta_1 = 10\gamma$.

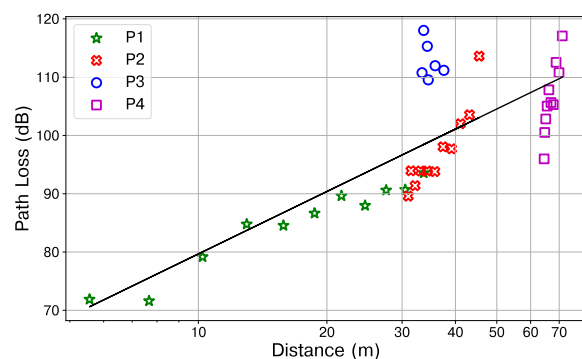
There are two methods to fit the data with this model. The first method considers β_0 and β_1 as the model parameters, which means they are determined by the maximum likelihood estimation. This method is called the FI model and it is equivalent to a simple linear regression problem. The other method considers only β_1 as the model parameter and it uses a theoretical value for β_0 such as the free-space path loss value at $d_0 = 1$ m. The model parameter β_1 is, of course, estimated by the maximum likelihood estimation. This method is called the CI model.

In the log-distance path loss model, path loss depends only on the distance between Tx and Rx, not on their multi-dimensional positions. Therefore, any two points that are located at the same distance from a fixed Tx position have the same expected path loss in this model. However, this property is not desirable in complex indoor environments.

Fig. 1 is a visualization of a partial dataset in the indoor corridor environment. In Fig. 1(a), the Tx position of this dataset is indicated by the star and the Rx positions are laid along walled corridors. According to the Rx positions of the dataset, we split the dataset into 4 groups - one for each passage (labeled as P1~P4). Fig. 1(b) visualizes the path loss of each data point. The x -axis is the log-distance between Tx and Rx. We see from the figure that all groups have different patterns.



(a)



(b)

FIGURE 1. (a) The layout of the indoor corridor environment. (b) Plot between the distance and path loss values. Black line is a fitted line of the data.

For example, the path loss values in P4 are plotted almost vertically while the path loss values in P2 and P3 behave differently even though their distances from Tx are almost the same. The reason for this is that the propagation distance is not really the same as the Euclidean distance between Tx and Rx. The dominant factors determining path loss in this walled corridor environment are the taxicab distance and the number of reflections during propagation, which are strongly related with the multi-dimensional structure between the points. Therefore, we conclude that the log-distance path loss model is not suitable for many practical cases, especially in complex indoor environments. It is clear that this data cannot be fitted into a single function of the log distance because it still fails to predict the path loss values for P2 and P3, for example. This is the reason why a multi-dimensional path loss model is required. In the next section, we explain the KNN regression model and propose our model based on Gaussian process regression.

III. MULTI-DIMENSIONAL PATH LOSS MODELS

As illustrated in Fig. 1, path loss cannot be correctly handled if it is considered as the function of a single variable d . To appropriately consider shadow fading due to spatial correlation, we consider a multi-dimensional regression method to develop a new path loss model. In this paper, we assume

that both Tx and Rx move simultaneously. This includes a lot of practical propagation scenarios including D2D and V2V communications.

The heights of Tx and Rx (denoted by z_{Tx} and z_{Rx} , respectively) are fixed in our experiment datasets and hence the input of a path loss function becomes 4 dimensional (2 dimensions for \mathbf{x}_{Rx} and 2 dimensions for \mathbf{x}_{Tx}). Note that the problem and model can be generalized to 6D easily, where the dataset contains different Tx and Rx heights. Then our objective is to construct a path loss function $PL(\mathbf{x}_{Tx}, \mathbf{x}_{Rx})$ to predict the path loss value at an arbitrary position, given a dataset $\{(\mathbf{x}_i, y_i)\}_{i=1}^N$ where \mathbf{x}_i is a 4-dimensional Tx-Rx position and y_i is the path loss value at the position of \mathbf{x}_i . We consider line-of-sight (LoS) and non-line-of-sight (nLoS) datasets separately and predict the LoS and nLoS path loss values separately.

Compared with the log-distance path loss model, a multi-dimensional path loss model has an advantage that it can predict path loss at any point by considering spatial correlation in more detail instead of considering the distance only. In a multi-dimensional path loss model, the objective is to construct a multivariate path loss function from a given data set and one possible approach is to simply use regression algorithms. In fact, there are existing multi-dimensional path loss models using regression algorithms, e.g., [41]. Among them, since the KNN regression model is recommended in [41] because of its prediction accuracy and the fastest computational time, we consider the KNN regression model for comparison purpose. In the following, we first explain the KNN regression model and then propose our model.

A. KNN REGRESION MODEL

The main idea of the KNN regression model is simple. Given the position of a test point \mathbf{x}_* and a pre-determined number K , the KNN regression model selects the K closest points \mathbf{x}_i , $1 \leq i \leq K$ in the training dataset and predicts the path loss value by the average of the path loss values at \mathbf{x}_i , $1 \leq i \leq K$ as follows:

$$PL = \frac{1}{K} \sum_{i=1}^K PL_i$$

where $PL_i (1 \leq i \leq K)$ is the path loss at position \mathbf{x}_i .

The original model in [41] uses 7 variables (Carrier frequency, Tx height, Rx position (3D), Tx-Rx distance, visibility (LoS/nLoS label)) as the input features, but we modify the model to use 5 variables (Tx position (2D), Rx position (2D), Tx-Rx distance) to make the model compatible with our dataset. Note that the heights of Tx and Rx in our experiments are fixed and are not needed to consider as the input features.

B. PROPOSED GPR-BASED PATH LOSS MODEL

We propose a GPR-based path loss model which is based on multi-dimensional GPR.¹ We construct our GPR-based path

loss model starting from decomposing PL into two terms:

$$PL(\mathbf{x}_{Tx}, \mathbf{x}_{Rx}) = f(\log_{10} d_{3D}(\mathbf{x}_{Tx}, \mathbf{x}_{Rx})) + g(\mathbf{x}_{Tx}, \mathbf{x}_{Rx}) \quad (3)$$

where we define a 3D distance function $d_{3D} : \mathbb{R}^2 \times \mathbb{R}^2 \rightarrow \mathbb{R}$ as

$$d_{3D}((x_1, y_1), (x_2, y_2)) = \sqrt{(x_1 - x_2)^2 + (y_1 - y_2)^2 + (z_{Rx} - z_{Tx})^2}. \quad (4)$$

In the model, $f(\log_{10} d_{3D}(\mathbf{x}_{Tx}, \mathbf{x}_{Rx}))$ represents the radial *mean* function that exploits the 1D structure of log-distance model to reflect the one-dimensional tendency and $g(\mathbf{x}_{Tx}, \mathbf{x}_{Rx})$ represents the *discrepancy* from the mean function that compensates the one-dimensional path loss prediction by using multi-dimensional spatial correlation in the environment. For each term, we further decompose it as follows:

$$f(\log_{10} d_{3D}) = P(\log_{10} d_{3D}) + GP_{1D}(\log_{10} d_{3D}) \quad (5)$$

and

$$g(\mathbf{x}_{Tx}, \mathbf{x}_{Rx}) = \sum_{q=1}^Q GP_{4D,q}(\mathbf{x}_{Tx}, \mathbf{x}_{Rx}). \quad (6)$$

Here's the description of each function given above:

- P is a linear function of $\log_{10} d_{3D}(\mathbf{x}_{Tx}, \mathbf{x}_{Rx})$ as in the log-distance path loss model. The coefficient in the function is considered as a hyperparameter in regression.
- GP_{1D} is a 1D Gaussian process with kernel (i.e., covariance)

$$k_{1D}((\mathbf{x}_{Tx}, \mathbf{x}_{Rx}), (\mathbf{x}'_{Tx}, \mathbf{x}'_{Rx})) = k_{SE}(\log_{10} d_{3D}(\mathbf{x}_{Tx}, \mathbf{x}_{Rx}), \log_{10} d_{3D}(\mathbf{x}'_{Tx}, \mathbf{x}'_{Rx})). \quad (7)$$

Since it is a smooth approximation for the mean function, we use a squared exponential (SE) kernel in this paper.

- $GP_{4D,q} (1 \leq q \leq Q)$ are 4D Gaussian processes. So we use a mixture of $Q (> 1)$ 4D Gaussian processes to consider various types of kernels in our model. Each $GP_{4D,q}$ has zero mean and kernel $k_{4D,q}$ which is specified later.

In summary, we use a Gaussian process whose mean function is a linear function (in log-distance), with kernel

$$k_{1D} + \sum_{q=1}^Q k_{4D,q} \quad (8)$$

to perform a regression for the path loss function $PL(\mathbf{x}_{Tx}, \mathbf{x}_{Rx})$. The hyperparameters for the mean function and kernels are trained simultaneously to maximize the log marginal likelihood function. Once the training is finished, we compute the posterior mean and variance of the path loss value at any point by using Bayesian inference. We then use the posterior mean value as the predicted path loss value at the point of interest.

¹Please refer to Appendix A for the mathematical details of GPR.

Alongside with the advantages of the multi-dimensional path loss model itself, we have additional advantages of our GPR-based path loss model as follows:

- The proposed model uses its special structure, that is, it is the sum of a 1D function $f(\log_{10} d_{3D})$ and a 4D function $g(\mathbf{x}_{Tx}, \mathbf{x}_{Rx})$. By training two functions simultaneously, the proposed model can predict path loss by capturing both local correlation and global tendency. In contrast, the KNN regression model determines its predicted value solely by the values of the K nearest points, which implies the prediction is performed locally and global tendency is completely neglected in prediction.
- Using the posterior mean and variance of the path loss value simultaneously, we can calculate the prediction interval of the path loss value at any position. The prediction interval can be also calculated in the log-distance path loss model because it has a Gaussian random variable χ_σ which corresponds to shadow fading. However, the GPR-based path loss model can provide much better prediction interval because shadow fading due to spatial correlation is taken into account while the log-distance path loss model assumes independent shadow fading.

To show that the advantages mentioned above actually appear in real environment, we conduct experiments to measure path loss in two indoor environments and compare prediction performance of the path loss models. Details about the measurement campaign are explained in Section IV. The experiment settings and results are provided in Section V, including comparison and analysis of prediction performance for the path loss models.

IV. MEASUREMENT CAMPAIGN

In this section, we briefly introduce channel sounder specifications used to measure indoor propagation channels, describe measurement environments, and explain how path loss is derived from CIR measurements.

A. SYSTEM DESCRIPTION

A wideband sliding correlation-based channel sounder is developed by the Electronics and Telecommunications Research Institute (ETRI), Korea. The hardware specifications including sounding signal parameters are summarized in Table 1 and the hardware is shown in Fig. 2. The Tx consists of a National Instruments (NI) digital baseband module PXIe-8135, a field programmable gate array (FPGA) module PXIe-7966, an radio frequency (RF) transmit adapter module NI 5793 that generates intermediate frequency (IF) signal at 2.3 GHz by using a 16-bit digital-to-analog converters (DACs), an RF upconverter, a single-pole four throw (SP4T) RF switch for four RF ports, and omnidirectional antennas connected to high power amplifiers (HPAs) at each port. The Rx consists of four omnidirectional antennas followed by low-noise amplifiers (LNAs), an SP4T RF switch for the RF ports, an RF downconverter, receiving RF adapter module NI 5792 that converts the analog received signal to digital

TABLE 1. Channel sounder specifications.

Parameters	Specification
Carrier frequency	4.1 GHz
Bandwidth	100 MHz
Number of Tx ports / used	4 / 1
Number of Rx ports / used	4 / 1
Tx EIRP	30 dBm
Chip sequence	m -sequence with length 1023
Chip waveform	SRRC pulse with roll-off factor 0.22
Chip rate	100 MHz

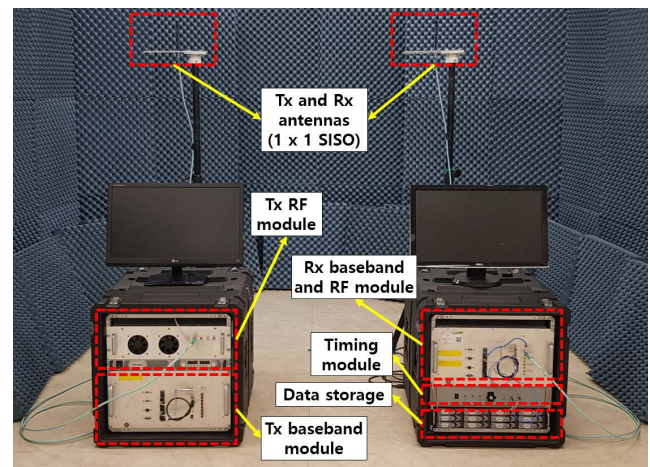


FIGURE 2. Channel sounder used for the measurement.

signal by using a 14-bit analog-to-digital converters (ADCs), an FPGA module PXIe-7966, and a digital baseband module PXIe-8135. As the measurement is for path loss rather than angular profiles, we terminated all ports but one port in the Tx and Rx respectively and used single-input single-output (SISO) system during the measurement.

The sounding signal is a square-root raised cosine (SRRC) pulse shaped 1023-length m -sequence with chip rate 100 MHz. The RF center frequency and bandwidth of the sounding signal is 4.1 GHz and 100 MHz, respectively. The effective isotropic radiated power (EIRP) of Tx is 30 dBm and the measurable Rx dynamic range of path loss is from 35 dB to 135 dB.

B. ENVIRONMENT DESCRIPTION

Indoor hotspot (InH) channel has long been measured and modeled due to its importance as one of the typical wireless communication environments [20], [23]. InH channel can be subdivided into indoor office and shopping mall according to 3GPP's definition [7]. We focus on the indoor office channel, which is commonly comprised of open cubicle areas, walled offices, and corridors. Among the components that compose the indoor office channel, corridor has to be separately investigated because of its special propagation characteristics. Thus, we conduct propagation channel measurements

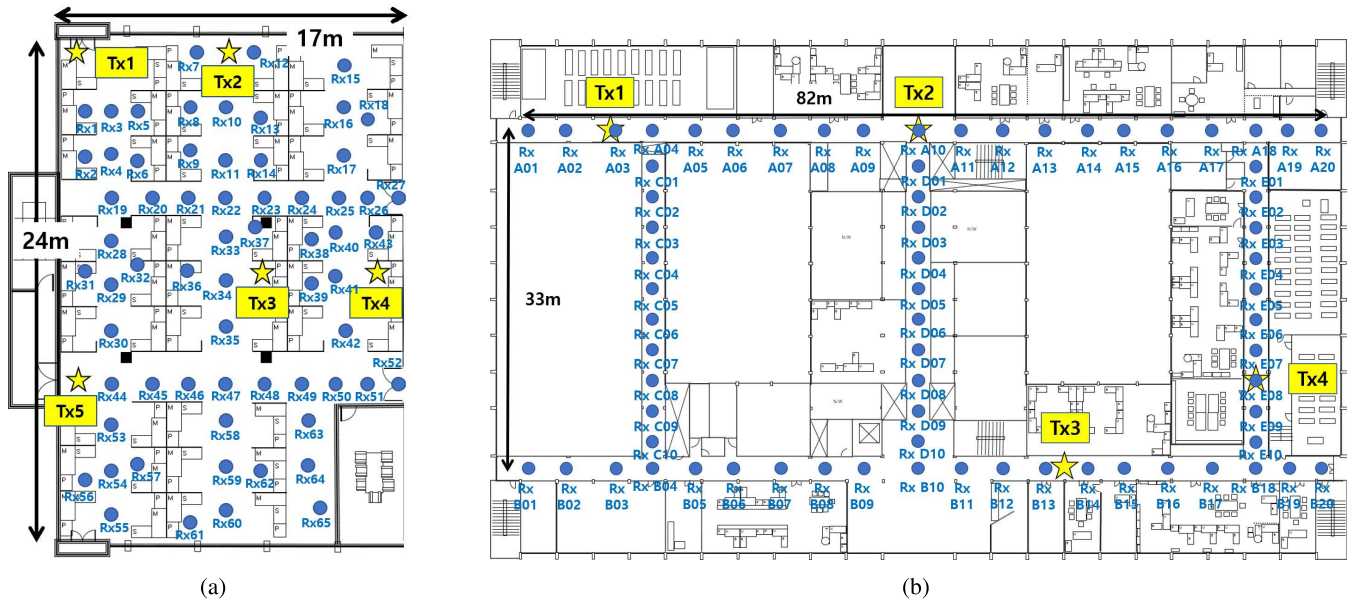


FIGURE 3. Measurement scenarios drawn on indoor environment layouts: (a) Office, (b) Corridor.

at indoor office and corridor, respectively. In this paper, office environment denotes the open cubicle areas without any walled offices or corridors. Fig. 3 shows the measurement scenarios at indoor office and corridor. The office size is 17m × 24m, and propagation channels between five Tx points and 65 Rx points are all measured. The heights of Tx and Rx antennas are 2.17m and 1.2m, respectively. The corridor environment is one floor of a building with size 82m × 33m. All propagation channels between four Tx points and 70 Rx points are measured, and the heights of Tx and Rx antennas are 2.1m and 1.2m, respectively.

Fig. 4 depicts the measurement campaigns. The office consists of various clutters such as pillars, bookshelves, computers, and desks that affect multi-path propagation. However, the corridor environment consists of concrete wall and some metal doors, which make the waveguide-like propagations. The two environments are very common in real-life, while it is considered hard to analyze their propagation properties because of the various obstacles resulting complex multipath propagation.

C. PATH LOSS EXTRACTION

All measured CIRs in Section IV-B are processed to extract respective wideband path loss values by using the method introduced in [45, Sec. 4.1.1.]. PDP at time instant t as a function of delay τ is derived from the CIR as

$$P(t, \tau) = |h(t, \tau)|^2, \tag{9}$$

where $h(t, \tau)$ denotes the CIR that represents the channel responses at each delay bin calibrated by Rx RF chain and antenna responses. Note that $h(t, \tau)$ in this subsection includes the Tx RF chain and antenna responses for convenience to calculate the received power. The PDPs in

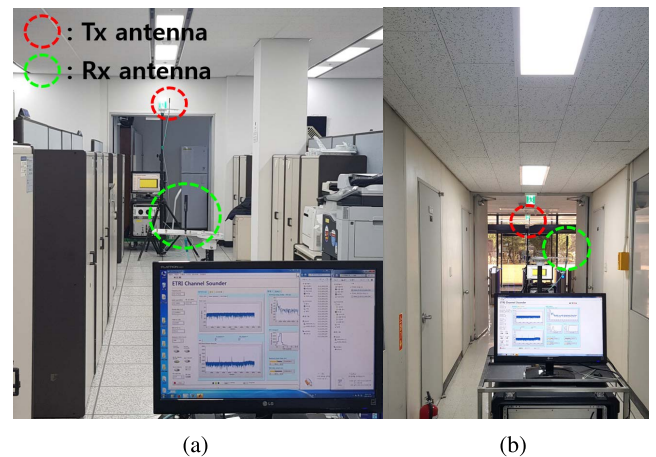


FIGURE 4. Measurement campaigns: (a) Office, (b) Corridor.

consecutive time domain can then be further averaged to reduce the noise floor level and small-scale time-varying effects as

$$P(\tau) = \frac{1}{N_t} \sum_{i=1}^{N_t} P(t_i, \tau), \tag{10}$$

where N_t is the number of consecutive CIRs and $P(t_i, \tau)$ is a PDP at time instance t_i . Then, we detect the delay corresponding to the highest peak power of the PDP as

$$\tau_m = \arg \max_{\tau} P(\tau) \tag{11}$$

and its power value $P(\tau_m)$, respectively. PDP is considered to be valid if and only if the largest power $P(\tau_m)$ is above 20 dB from the noise floor level, and further used for path loss calculation. Finally, the received power and path loss are

extracted from the summation of the PDP over delay domain as

$$P_{Rx} = \sum_{i=1}^{N_\tau} P(\tau_i) \quad (12)$$

and

$$PL = 10 \log_{10}(P_{Tx}) - 10 \log_{10}(P_{Rx}) \quad (13)$$

respectively, where i and N_τ represent the indices and total numbers of delay bins that have power larger than $10 \log_{10}(P(\tau_m)) - 20$ dB, respectively, and P_{Tx} is the Tx EIRP in linear scale. This path loss value is used in the dataset for the path loss models.

In the office environment, we use 323 sets of path loss data between 5 Tx points and 65 Rx points where we exclude some nearby Tx-Rx locations. In the corridor environment, we use 252 sets of path loss data between 4 Tx points and 70 Rx points where we exclude some nearby Tx-Rx locations and the locations whose largest powers in PDP do not exceed 20 dB from the noise floor level as mentioned in Section V-C.

V. VALIDATION AND RESULTS

Using the measured path loss values in the previous section, we compare the path loss models in this section. The method used for comparison is leave-one-out cross validation (LOOCV) which is a method to check out whether a given model predicts a single observation from a dataset excluding the single observation. LOOCV is widely used to evaluate prediction performance of machine learning algorithms and hence is suitable for our experiments. We summarize the settings that we use for comparison before providing with comparison results and analysis.

A. DETAILS IN THE SETTINGS

We compare the GPR-based path loss model with the log-distance path loss model and the KNN regression model. In this subsection, we explain the error metrics and implementation methods of all models in comparison.

1) ERROR METRICS

We consider 4 scenarios according to the environments - office and corridor - and the LoS/nLoS labels. For each scenario, we obtain an experimental dataset by using the methodologies in the previous section. We use the leave-one-out (LOO) cross-validation: For a dataset $\{(\mathbf{x}_i, y_i)\}_{i=1}^N$, we calculate the predicted value \hat{y}_i (called leave-one-out predicted value) at the position \mathbf{x}_i by a model which is trained from the whole dataset except the point (\mathbf{x}_i, y_i) . The LOO cross-validation is usually used to evaluate the generalization performance of a learned model (i.e., to check if the model prevents the overfitting issue).

We compare prediction performance of the path loss models by using two metrics based on LOO cross-validation - LOO mean-squared error (LOO-MSE) and LOO maximum absolute error (LOO-MAE). Let \hat{y}_i be the LOO predicted

value at the position \mathbf{x}_i . Then the LOO-MSE is defined by

$$\text{MSE} = \sqrt{\frac{1}{N} \sum_{i=1}^N (y_i - \hat{y}_i)^2} \quad (14)$$

and the LOO-MAE is defined by

$$\text{MAE} = \max_{i=1}^N |y_i - \hat{y}_i|. \quad (15)$$

Both metrics estimate the discrepancy between LOO predicted values and true (measured) values, but the LOO-MSE focuses on how a model predicts well in average, while the LOO-MAE focuses on the worst case performance of a model in prediction. As a high error at a certain position is likely to cause a serious connection problem at the position in real-world applications, minimizing the LOO-MAE is as important as minimizing the average error (LOO-MSE).

2) LOG-DISTANCE PATH LOSS MODEL

For the log-distance path loss model we apply both the FI model and the CI model. Hence, the LOO-MSE values for both models are provided. We use the 1 m free-space path loss value of 44.70 dB in the CI model (49.43 dB in 7.075 GHz environment given later). We develop a simple code with Python [46] to implement this model.

3) KNN REGRESSION MODEL

For the KNN regression model, we use the corresponding library of Scipy [47] for its implementation. The performance of the model is significantly affected by the selection of K , the number of the closest neighbors. The use of $K = 3$ yields the best results in our experiments.

4) GPR-BASED PATH LOSS MODEL

In our experiment, we use $Q = 3$ and the following four mixture kernels:

- SE : Mixture of three SE kernels.
- M12 : Mixture of three Matérn 1/2 kernels.
- M32 : Mixture of three Matérn 3/2 kernels.
- Mix : Mixture of SE, Matérn 1/2, and Matérn 3/2 kernels.

The details of the above kernels are provided in Appendix B. We implement the GPR-based path loss model using Python and GPFLOW [48] which is an extensive Gaussian process library based on Tensorflow [49]. The Limited-memory Broyden-Feltcher-Goldfarb-Shannon for Bounded variables (L-BFGS-B) [50] algorithm is used to maximize the log marginal likelihood, and we use the default parameter values used in the Scipy optimizer. We use the following simple algorithms for the initial values of the hyperparameters:

- The default values of the initial hyperparameters are vectors of 1.0, i.e., [1.0, 1.0, 1.0, 1.0], etc.
- To ensure that Q copies of GP are trained differently, we add noises to the initial lengthscales of individual Gaussian processes.

TABLE 2. The LOO-MSE of path loss in the experiment environments with path loss models.

LOO-MSE(dB)		Office		Corridor	
		LoS	nLoS	LoS	nLoS
Log-Distance	FI	2.2394	2.1479	3.3240	6.4335
	CI	2.3998	2.6003	3.3524	6.5482
KNN		2.1630	2.2449	3.2830	4.1954
GPR (Proposed)	SE	2.1253	2.0410	2.6541	3.2821
	M12	2.0802	1.8781	2.8514	3.0897
	M32	2.1053	1.8520	2.7094	3.1833
	Mix	2.1021	1.8812	2.7803	3.1709

TABLE 3. The LOO-MAE of path loss in the experiment environments with path loss models.

LOO-MAE(dB)		Office		Corridor	
		LoS	nLoS	LoS	nLoS
Log-Distance	FI	6.6331	5.5721	9.1822	21.6068
	CI	7.2274	9.4983	9.6889	21.3375
KNN		6.7124	5.9069	8.0746	12.5145
GPR (Proposed)	SE	6.0879	5.6257	6.5476	10.0281
	M12	6.6032	4.5711	7.0682	9.9378
	M32	5.8631	4.3484	6.9738	10.6987
	Mix	6.0068	4.9490	7.1290	9.6956

- Sometimes the optimizer fails to converge and yields an error in GPFlow. This usually happens when the initial lengthscales are too small. In this case, we doubles the initial lengthscales and retry.

Using the above models, we compare the prediction performance of the path loss models. Table 2 and 3 represent the error metrics in path loss prediction for four different scenarios, LoS/ nLoS scenarios in two environments.

B. LOG-DISTANCE PATH LOSS MODEL

We first analyze the LOO-MSE of the log-distance path loss model. From its definition, the LOO-MSE of the log-distance path loss model is close to σ which is the standard deviation of shadow fading in the model. As this value gets large, the environment is considered complex to analyze in the model.

In the office environment, the obstacles are placed in orders so the multipath components appear very smoothly. This results in relatively low LOO-MSE in every model. In the log-distance path loss model, the lowest LOO-MSE are 2.2394 and 2.1479 for LoS and nLoS, respectively.

In the corridor environment, on the other hand, the propagation nature changes very extremely. This is the observation that is pointed out in Section II. The observation is supported by relatively high LOO-MSE in the log-distance path loss model. The lowest LOO-MSEs are 3.3240 and 6.4335 in LoS and nLoS, respectively. Especially, the log-distance path loss model shows poor performance in the corridor nLoS

environment because of its strong multi-dimensional correlations as pointed out in Fig. 1.

The LOO-MAE in Table 3 also shows a similar trend to the LOO-MSE in Table 2, but the values of the error metric get much larger as it represents the maximum error. In the corridor nLoS scenario, for example, the LOO-MAE becomes extremely large like 21 dB. Such a high error implies that the log-distance path loss model is easy to fail to predict path loss at certain points, even if the measurement data values exist at points nearby.

C. KNN REGRESSION MODEL

The LOO-MSE values in the KNN regression model are similar to those in the log-distance path loss model as shown in Table 2, except for the nLoS corridor environment where we see a substantial improvement (34.8 % smaller LOO-MSE) compared with the log-distance path loss model. As previously mentioned in Fig. 1, the nLoS corridor environment has strong multi-dimensional spatial correlation. So, this shows that even the simplest consideration of multi-dimensional spatial correlation can be effective in a complex propagation environment.

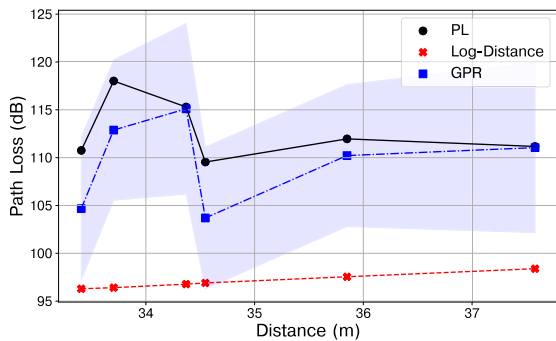
D. PROPOSED GPR-BASED PATH LOSS MODEL

Our GPR-based path loss model outperforms the log-distance path loss model for all kernels and scenarios as shown in Table 2 and Table 3 except for one case (SE kernel, nLoS office environment).

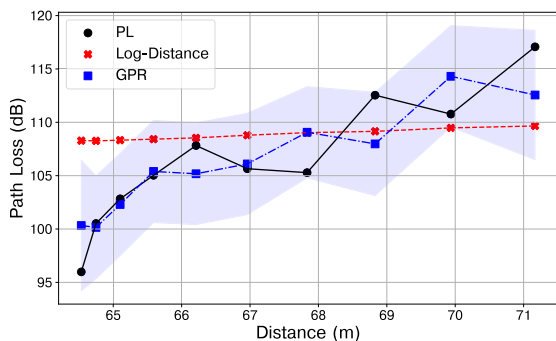
To see the ability of capturing multi-dimensional spatial correlation of path loss in the GPR-based path loss model, we provide in Fig. 5 with the LOO values in the log-distance path loss model and the GPR-based path loss model along one passage. As shown in the figure, we see that the GPR-based path loss model outperforms the log-distance path loss model. As pointed out in Fig. 1, the Euclidean distances of the points are not much different in this case. Therefore, the log-distance path loss model provides with predicted values that are not significantly different. In contrast, the GPR-based path loss model makes predictions closer to the actual path loss data because spatial correlation is captured well by introducing Gaussian processes. This shows that the GPR-based path loss model can predict path loss better than the log-distance path loss model.

One more thing to worth mentioning in Fig. 5 is that the GPR-based path loss model provides with prediction intervals with high reliability. That is, as shown in the figure, we easily see that the 95% prediction intervals of the LOO values cover all true (measured) path loss values.

When we compare the KNN regression model with our GPR-based path loss model, Table 2 and Table 3 show that our GPR-based path loss model outperforms the KNN regression model in most cases. In particular, it is worth mentioning that our GPR-based path loss model has 26.4% smaller LOO-MSE error than the KNN regression model in the nLoS corridor environment. This shows that we can improve prediction performance by introducing Gaussian processes.



(a)



(b)

FIGURE 5. The LOO values of the log-distance and GPR-based path loss models in the passage P3 (a) and P4 (b) introduced in Fig. 1. Matérn 1/2 kernel is used in the GPR-based path loss model. The shaded region represents the 95% prediction interval of predicted path loss in the GPR-based path loss model.

Unlike the KNN regression model which performs similar to the log-distance path loss model in the office environment, our GPR-based path loss model provide consistently better performance in all cases. This implies that our GPR-based path loss model is both accurate and stable, even for small datasets as in our experiments.

To see the performance improvement more clearly for our GPR-based path loss model, we plot in Fig. 6 the distribution of the LOO Error for each path loss model in the nLoS corridor environment. From the figure we see that the most probabilities of the LOO Error are located closer to 0 in our GPR-based path loss model than in the other path loss models.

Choosing a good kernel to explain a given dataset well is often an important issue when applying Gaussian processes and usually called the kernel selection problem. In our experiments we try a number of different mixture kernels and see in Table 2 and Table 3 that the results are quite similar for all kernels. So, even though there still exists a possibility for performance improvement by choosing a better kernel, from our extensive experiments we believe the resulting performance of other kernels would be not much different from ours in the tables. In fact, we can conclude from our experiments that a mixture of SE kernels provides with good results and hence is a good choice for the proposed path loss model.

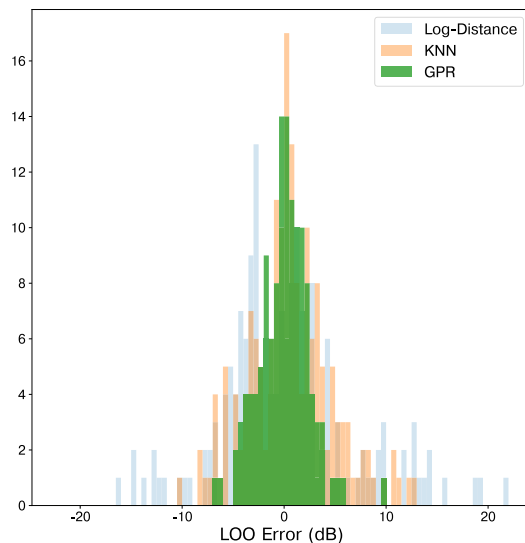


FIGURE 6. The histogram of LOO errors in the nLoS corridor environment. The FI model is used for the log-distance path loss model. Matérn 1/2 kernel is used in the GPR-based path loss model.

TABLE 4. The pseudo log-likelihood value for each kernel in the GPR-based path loss model.

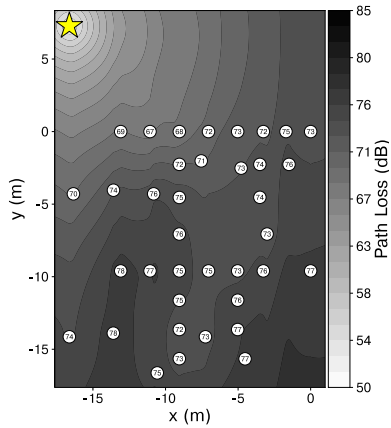
PLL	Office		Corridor	
	LoS	nLoS	LoS	nLoS
SE	-296.8078	-291.6431	-168.1124	-389.7659
M12	-292.6156	-277.8451	-174.1934	-381.9334
M32	-295.4998	-275.1101	-168.6910	-390.1596
Mix	-295.2924	-278.2922	-172.6007	-386.1406

Even the kernel selection problem in GPR can be automated by introducing an auxiliary metric like pseudo log-likelihood (PLL). It is the estimated value of the log-likelihood, which means how much the dataset is probable in the given GP model. It is calculated by the following formula

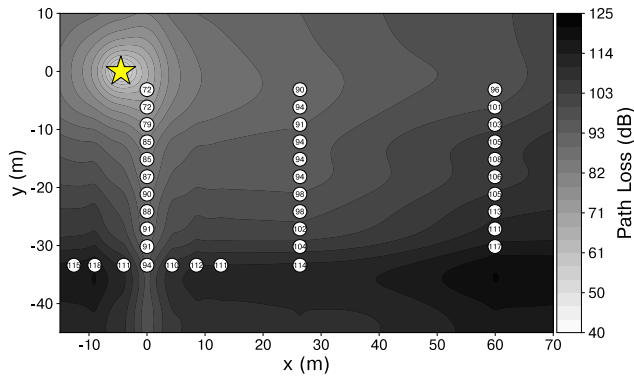
$$PLL = \sum_{i=1}^N -\frac{1}{2} \log \sigma_i^2 - \frac{(y_i - \mu_i)^2}{\sigma_i^2} - \frac{1}{2} \log 2\pi \quad (16)$$

where μ_i and σ_i^2 are the mean and variance of the LOO predicted value at the position \mathbf{x}_i , respectively. Table 4 provides with the calculated PLL values for the selected kernels. Note that the optimal kernels based on PLL result in the lowest LOO-MSE values in Table 2. This shows that PLL is a good candidate of the metric for automated kernel selection.

We would like to mention that our GPR-based path loss model can be also used to simulate path loss in a given environment after training the measurement data from the environment. Fig. 7 provides with the predicted means of nLoS path losses in the GPR-based path loss model in the office and corridor environments. We see that the trained function PL demonstrates path loss well and predicts its spatial correlation in the environments as well. For example, we clearly see in Fig. 7 that the predicted path loss is lower



(a)



(b)

FIGURE 7. Simulation results for the GPR-based path loss model. (a) Simulation for office Tx1 nLoS path loss with M12 kernel. (b) Simulation for corridor Tx1 nLoS path loss with Mix kernel. Stars indicate Tx positions. White circles indicate Rx positions, and the numbers given in the circles are the true path loss values. Brighter shadow implies smaller path loss.

than the surroundings in the left and middle passages of the office environment or the left passage in the corridor environment. Both results can be easily expected from the actual diagrams provided in Fig. 3. The importance of this observation is that we don't need any information on the environment other than the path loss values in our proposed model.

To show that our proposed model also works well in various frequencies, we perform an additional measurement campaign at a higher frequency (7.075 GHz) with the same channel sounder settings specified in Table 1. In the office environment, 323 sets of path loss data are used as in the 4.1GHz case, and in the corridor environment, 208 sets of path loss data are used. In Table 5 and Table 6, we provide with the LOO-MSE and LOO-MAE of each path loss model in the 7.075 GHz environment. The tables show a similar trend to Table 2 and Table 3, that the proposed GPR-based path loss model shows consistently lower LOO-MSE and LOO-MAE compared with the log-distance path loss model and the KNN regression model. Based on our experimental results, we expect that the proposed model provides

TABLE 5. The LOO-MSE of path loss in the experiment environments with path loss models at 7.075 GHz.

LOO-MSE(dB)		Office		Corridor	
		LoS	nLoS	LoS	nLoS
Log-Distance	FI	2.0820	2.2342	2.8745	4.7839
	CI	2.4110	2.5099	2.8851	4.8063
KNN		2.2568	2.3465	3.3543	4.1086
GPR (Proposed)	SE	1.8511	2.0465	2.8043	3.4994
	M12	2.0063	2.0168	2.8213	3.3543
	M32	1.9476	2.0410	2.8118	3.3524
	Mix	1.9878	2.0229	2.7983	3.3589

TABLE 6. The LOO-MAE of path loss in the experiment environments with path loss models at 7.075 GHz.

LOO-MAE(dB)		Office		Corridor	
		LoS	nLoS	LoS	nLoS
Log-Distance	FI	5.3857	8.0726	7.6811	13.7092
	CI	8.4387	12.9239	8.0723	13.7102
KNN		6.4122	8.5786	9.4168	13.8054
GPR (Proposed)	SE	4.7824	5.8912	6.9415	10.8627
	M12	4.8434	6.0736	7.0404	10.9327
	M32	4.8567	5.8405	7.0046	10.3342
	Mix	4.9685	5.7442	6.9415	9.8918

consistently good performance and can be used for any general measurement campaign on path loss, as it does not require any specific assumption on the dataset.

VI. CONCLUSION

In this paper, a multi-dimensional GPR-based path loss model is proposed to estimate path loss. In our model, the path loss function is divided into the radial mean function and Gaussian processes representing shadow fading. The parameters of the Gaussian processes and the coefficients determining the mean function are estimated by maximizing the log marginal likelihood function. We consider two indoor environments to validate the proposed model and show that our model outperforms the existing models, e.g., the log-distance path loss model and the KNN regression model. The strength of the proposed model is that it has a special structure consisting of a radial mean function and a local shadowing term, which makes the prediction more accurate. In addition, we see that it can provide the prediction interval of the predicted path loss value and be used for the simulation as well. The simulation results can be used to optimize the positions and channel gains of the antennas with relatively low cost.

While the proposed model is the first approach to consider the multi-dimensional structure in path loss to the best of authors' knowledge, verifying and improving it are the good directions of our future works. Obviously, the proposed model should be tested and verified in more various

environments, including outdoor and large-scale environments. Moreover, while the proposed model trains LoS/nLoS path losses independently, it can be improved to predict both at once using, e.g., multi-output Gaussian process (MOGP). GPR or other machine learning-based regression methods can be also applied to predict raw CIR data with respect to multi-dimensional Tx-Rx position, instead of path loss data. This approach can be a great extension of the proposed model because other channel parameters like delay spread can be also predicted simultaneously.

APPENDIX A GAUSSIAN PROCESS REGRESSION

The regression problem is to predict a continuous target variable $y \in \mathbb{R}$ corresponding to an input variable $\mathbf{x} \in \mathbb{R}^d$. Let $\mathcal{D} = \{(\mathbf{x}_i, y_i) : \mathbf{x}_i \in \mathcal{X}, y_i \in \mathbb{R}, i = 1, \dots, n\}$ be a given dataset.

Gaussian process (GP) is a distribution of the real-valued function $f : \mathbb{R}^d \rightarrow \mathbb{R}$. The distribution $p(f)$, or simply f is a Gaussian process if and only if for any finite subset $\{\mathbf{x}_1, \dots, \mathbf{x}_n\} \subset \mathbb{R}^d$, the marginal distribution over the finite subset $\{f(\mathbf{x}_1), \dots, f(\mathbf{x}_n)\} \subset \mathbb{R}^d$ is a multivariate Gaussian distribution. GP is completely determined from two functions $m : \mathbb{R}^d \rightarrow \mathbb{R}$ and $k : \mathbb{R}^d \times \mathbb{R}^d \times \mathbb{R}$, where

$$\begin{aligned} m(\mathbf{x}) &= \mathbb{E}_{f \sim p}[f(\mathbf{x})] \\ k(\mathbf{x}, \mathbf{x}') &= \mathbb{E}_{f \sim p}[(f(\mathbf{x}) - m(\mathbf{x}))(f(\mathbf{x}') - m(\mathbf{x}'))]. \end{aligned} \quad (17)$$

$m(\mathbf{x})$ is called the mean function and $k(\mathbf{x}, \mathbf{x}')$ is called the kernel function of GP.

Gaussian process regression (GPR) [52] is a regression model using Gaussian process, as its name states. It is a kind of Bayesian inference. Bayesian inference is conducted as follows: We give a prior distribution $p(\mathbf{f})$ of the function \mathbf{f} and use the Bayes' rule

$$p(\mathbf{f}|\mathbf{X}, \mathbf{y}) = \frac{p(\mathbf{y}|\mathbf{X}, \mathbf{f})p(\mathbf{f})}{p(\mathbf{y}|\mathbf{X})} \quad (18)$$

to derive the posterior distribution $p(\mathbf{f}|\mathbf{X}, \mathbf{y})$ of \mathbf{f} . Therefore, the result of GPR appears in terms of distribution, not in terms of a single value. To select a representative value for prediction, we usually use the mean of the posterior distribution.

The GPR model assumes each output y_i is the sum of $f(\mathbf{x}_i)$ and independent Gaussian noise $\epsilon_i \sim \mathcal{N}(0, \sigma_n^2)$. We give a prior distribution of f by the mean function $m(\mathbf{x})$ and kernel $k(\mathbf{x}, \mathbf{x}')$. The prediction in GPR is conducted by calculating the conditional distribution. Suppose that we want to predict the outputs in the test points $\mathbf{X}_* = [\mathbf{x}_1, \dots, \mathbf{x}_m]$. We first consider the joint probability distribution of $\mathbf{y} = [y_1, \dots, y_m]^\top$ and $\mathbf{f}_* = [f(\mathbf{x}_1), \dots, f(\mathbf{x}_m)]^\top$ by

$$\begin{bmatrix} \mathbf{y} \\ \mathbf{f}_* \end{bmatrix} \sim \mathcal{N} \left(\begin{bmatrix} \mathbf{m}(\mathbf{X}) \\ \mathbf{m}(\mathbf{X}_*) \end{bmatrix}, \begin{bmatrix} \mathbf{K}(\mathbf{X}, \mathbf{X}) + \sigma_n^2 \mathbf{I}_n & \mathbf{K}(\mathbf{X}, \mathbf{X}_*) \\ \mathbf{K}(\mathbf{X}_*, \mathbf{X}) & \mathbf{K}(\mathbf{X}_*, \mathbf{X}_*) \end{bmatrix} \right) \quad (19)$$

where

$$\begin{aligned} \mathbf{m}([\mathbf{a}_i]_{1 \leq i \leq k}) &= [m(\mathbf{a}_i)]_{1 \leq i \leq k}, \\ \mathbf{K}([\mathbf{a}_i]_{1 \leq i \leq k}, [\mathbf{b}_i]_{1 \leq i \leq l}) &= [k(\mathbf{a}_i, \mathbf{b}_j)]_{1 \leq i \leq k, 1 \leq j \leq l}, \end{aligned} \quad (20)$$

and \mathbf{I}_n is the $n \times n$ identity matrix. Then, we use the Bayes' rule to calculate the conditional distribution of \mathbf{f}_* by

$$\mathbf{f}_* | \mathcal{D}, \mathbf{X}_* \sim \mathcal{N}(\bar{\mathbf{f}}_*, \text{cov}(\mathbf{f}_*)) \quad (21)$$

where

$$\bar{\mathbf{f}}_* = \mathbf{m}(\mathbf{X}_*) + \mathbf{K}(\mathbf{X}_*, \mathbf{X}) \mathbf{K}_n^{-1} (\mathbf{y} - \mathbf{m}(\mathbf{X})), \quad (22)$$

$$\text{cov}(\mathbf{f}_*) = \mathbf{K}(\mathbf{X}_*, \mathbf{X}_*) - \mathbf{K}(\mathbf{X}_*, \mathbf{X}) \mathbf{K}_n^{-1} \mathbf{K}(\mathbf{X}, \mathbf{X}_*). \quad (23)$$

Here, $\mathbf{K}_n = \mathbf{K}(\mathbf{X}, \mathbf{X}) + \sigma_n^2 \mathbf{I}_n$. Then we use $\bar{\mathbf{f}}_*$ as the predicted values of \mathbf{f}_* and use $\text{cov}(\mathbf{f}_*)$ as the variances of the prediction.

We need to determine the kernel function k when GPR is applied. The most popular choice of k is the squared exponential (SE) kernel

$$k(\mathbf{x}, \mathbf{x}') = \sigma_s^2 \exp \left(-\frac{|\mathbf{x} - \mathbf{x}'|^2}{2\ell^2} \right) \quad (24)$$

where σ_s^2 determines the amplitude of the kernel and ℓ is called the lengthscale. The SE kernel is usually used to represent a smooth function. To represent functions with weaker regularity, the Matérn kernel

$$\begin{aligned} k(\mathbf{x}, \mathbf{x}') &= \sigma_s^2 \frac{1-\nu}{\Gamma(\nu)} \left(\frac{\sqrt{2\nu}|\mathbf{x} - \mathbf{x}'|}{\ell} \right)^\nu \\ &\times K_\nu \left(\frac{\sqrt{2\nu}|\mathbf{x} - \mathbf{x}'|}{\ell} \right) \end{aligned} \quad (25)$$

is considered. Here, σ_s^2 is the amplitude, ℓ is the lengthscale, and ν represents the regularity of the kernel. K_ν in the formula is the modified Bessel function of the second kind. As ν gets bigger, the resulting Gaussian process becomes smoother. The Matérn kernel with $\nu = \frac{1}{2}$ is called Matérn 1/2 kernel and the Matérn kernel with $\nu = \frac{3}{2}$ is called Matérn 3/2 kernel.

All of the kernels mentioned above are represented by the radial term $|\mathbf{x} - \mathbf{x}'|^2/\ell^2$, and it is weighted equally for any direction. Such kernel is called an isotropic kernel. In contrast, we use heterotropic kernels for Gaussian processes which are asymmetric in different dimensions. In heterotropic kernels, the radial term $|\mathbf{x} - \mathbf{x}'|^2/\ell^2$ in the isotropic kernel is replaced by

$$\sum_{i=1}^d \frac{(x_i - x'_i)^2}{\ell_i^2}. \quad (26)$$

In this case, the lengthscales form a vector $[\ell_1, \dots, \ell_d]^\top$, which represent different weights for input dimensions.

The mixture kernel is also widely used since it can reproduce various shapes of functions by summing several kernels. The mixture kernel is used in our experiments, too.

Before the inference step, we should determine the hyperparameters of the GPR model. In general, these hyperparameters (usually denoted by θ) are calculated by maximizing the log marginal likelihood function

$$\begin{aligned} \log p(\mathbf{y}|\mathbf{X}, \theta) = & -\frac{1}{2}(\mathbf{y} - \mathbf{m}(\mathbf{X}))^\top \mathbf{K}_n^{-1}(\mathbf{y} - \mathbf{m}(\mathbf{X})) \\ & - \frac{1}{2} \log |\mathbf{K}(\mathbf{X}, \mathbf{X}) + \sigma_n^2 \mathbf{I}_n| - \frac{n}{2} \log 2\pi. \end{aligned} \quad (27)$$

We usually use the gradient descent method to maximize this function.

REFERENCES

- [1] *Technical Specification Group Radio Access Network; NR; Physical Channels and Modulation*, document 3GPP TS 38.211 v16.2.0, Release 16, Jul. 2020.
- [2] N. Costa and S. Haykin, *Multiple-Input Multiple-Output Channel Models: Theory and Practice*. Hoboken, NJ, USA: Wiley, 2010.
- [3] S. Salous, *Radio Propagation Measurements and Channel Modelling*. Hoboken, NJ, USA: Wiley, 2013.
- [4] G. L. Turin, F. D. Clapp, T. L. Johnston, S. B. Fine, and D. Lavry, "A statistical model of urban multipath propagation," *IEEE Trans. Veh. Technol.*, vol. VT-21, no. 1, pp. 1–9, Feb. 1972.
- [5] A. A. M. Saleh and R. A. Valenzuela, "A statistical model for indoor multipath propagation," *IEEE J. Sel. Areas Commun.*, vol. JSAC-5, no. 2, pp. 128–137, Feb. 1987.
- [6] L. Liu, C. Oestges, J. Poutanen, K. Haneda, P. Vainikainen, F. Quitin, F. Tufvesson, and P. De Doncker, "The COST 2100 MIMO channel model," *IEEE Wireless Commun.*, vol. 19, no. 6, pp. 92–99, Dec. 2012.
- [7] *Technical Specification Group Radio Access Network; Study on Channel Model for Frequencies From 0.5 to 100 GHz*, document 3GPP TR 38.901 V16.1.0, Release 16, Dec. 2019.
- [8] P. Kyösti, "WINNER II channel models," Eur. Commission, Brussels, Belgium, Tech. Rep. D1.1.2, Feb. 2008.
- [9] C. Huang, R. Wang, P. Tang, R. He, B. Ai, Z. Zhong, C. Oestges, and A. F. Molisch, "Geometry-cluster-based stochastic MIMO model for vehicle-to-vehicle communications in street canyon scenarios," *IEEE Trans. Wireless Commun.*, vol. 20, no. 2, pp. 755–770, Feb. 2021.
- [10] A. F. Molisch, H. Asplund, R. Heddergott, M. Steinbauer, and T. Zwick, "The COST259 directional channel model—Part I: Overview and methodology," *IEEE Trans. Wireless Commun.*, vol. 5, no. 12, pp. 3421–3433, Dec. 2006.
- [11] H. Asplund, A. A. Glazunov, A. F. Molisch, K. I. Pedersen, and M. Steinbauer, "The COST 259 directional channel model—Part II: Macrocells," *IEEE Trans. Wireless Commun.*, vol. 5, no. 12, pp. 3434–3450, Dec. 2006.
- [12] P. Kyösti, J. Lehtomäki, J. Medbo, and M. Latva-Aho, "Map-based channel model for evaluation of 5G wireless communication systems," *IEEE Trans. Antennas Propag.*, vol. 65, no. 12, pp. 6491–6504, Dec. 2017.
- [13] J. Weng, X. Tu, Z. Lai, S. Salous, and J. Zhang, "Indoor massive MIMO channel modelling using ray-launching simulation," *Int. J. Antennas Propag.*, vol. 2014, pp. 1–13, Sep. 2014.
- [14] F. Hossain, T. Geok, T. Rahman, M. Hindia, K. Dimiyati, S. Ahmed, C. Tso, and N. A. Rahman, "An efficient 3-D ray tracing method: Prediction of indoor radio propagation at 28 GHz in 5G network," *Electronics*, vol. 8, no. 3, p. 286, Mar. 2019.
- [15] A. I. Sulyman, A. T. Nassar, M. K. Samimi, G. R. MacCartney, Jr., T. S. Rappaport, and A. Alsanie, "Radio propagation path loss models for 5G cellular networks in the 28 GHz and 38 GHz millimeter-wave bands," *IEEE Commun. Mag.*, vol. 52, no. 9, pp. 78–86, Sep. 2014.
- [16] J. Y. Lee, S. J. Bae, Y. M. Kwon, and M. Y. Chung, "Interference analysis for femtocell deployment in OFDMA systems based on fractional frequency reuse," *IEEE Commun. Lett.*, vol. 15, no. 4, pp. 425–427, Apr. 2011.
- [17] M. Rebato, J. Park, P. Popovski, E. D. Carvalho, and M. Zorzi, "Stochastic geometric coverage analysis in mmWave cellular networks with realistic channel and antenna radiation models," *IEEE Trans. Commun.*, vol. 67, no. 5, pp. 3736–3752, May 2019.
- [18] J. B. Andersen, T. S. Rappaport, and S. Yoshida, "Propagation measurements and models for wireless communications channels," *IEEE Commun. Mag.*, vol. 33, no. 1, pp. 42–49, Jan. 1995.
- [19] T. S. Rappaport, F. Gutierrez, Jr., E. Ben-Dor, J. N. Murdock, Y. Qiao, and J. I. Tamir, "Broadband millimeter-wave propagation measurements and models using adaptive-beam antennas for outdoor urban cellular communications," *IEEE Trans. Antennas Propag.*, vol. 61, no. 4, pp. 1850–1859, Apr. 2013.
- [20] K. Haneda, L. Tian, H. Asplund, J. Li, Y. Wang, D. Steer, C. Li, T. Balercia, S. Lee, Y. Kim, and A. Ghosh, "Indoor 5G 3GPP-like channel models for office and shopping mall environments," in *Proc. IEEE Int. Conf. Commun. Workshops*, May 2016, pp. 694–699.
- [21] G. R. MacCartney and T. S. Rappaport, "Rural macrocell path loss models for millimeter wave wireless communications," *IEEE J. Sel. Areas Commun.*, vol. 35, no. 7, pp. 1663–1677, Jul. 2017.
- [22] S. Hur, S. Baek, B. Kim, J. Park, A. F. Molisch, K. Haneda, and M. Peter, "28 GHz channel modeling using 3D ray-tracing in urban environments," in *Proc. 9th Eur. Conf. Antennas Propag. (EuCAP)*, May 2015, pp. 1–5.
- [23] S. Sangodoyin, V. Kristem, A. F. Molisch, R. He, F. Tufvesson, and H. M. Behairy, "Statistical modeling of ultrawideband MIMO propagation channel in a warehouse environment," *IEEE Trans. Antennas Propag.*, vol. 64, no. 9, pp. 4049–4963, Sep. 2016.
- [24] *Guidelines for Evaluation of Radio Interface Technologies for IMT-2020*, document ITU-R M.2412-0, Geneva, Switzerland, Oct. 2017.
- [25] T. S. Rappaport, G. R. MacCartney, M. K. Samimi, and S. Sun, "Wideband millimeter-wave propagation measurements and channel models for future wireless communication system design," *IEEE Trans. Commun.*, vol. 63, no. 9, pp. 3029–3056, Sep. 2015.
- [26] S. Sun, T. S. Rappaport, T. A. Thomas, A. Ghosh, H. C. Nguyen, I. Z. Kovacs, I. Rodriguez, O. Koymen, and A. Partyka, "Investigation of prediction accuracy, sensitivity, and parameter stability of large-scale propagation path loss models for 5G wireless communications," *IEEE Trans. Veh. Technol.*, vol. 65, no. 5, pp. 2843–2860, May 2016.
- [27] M. Shafi, J. Zhang, H. Tataria, A. F. Molisch, S. Sun, T. S. Rappaport, F. Tufvesson, S. Wu, and K. Kitao, "Microwave vs. millimeter-wave propagation channels: Key differences and impact on 5G cellular systems," *IEEE Commun. Mag.*, vol. 56, no. 12, pp. 14–20, Dec. 2018.
- [28] A. Karttunen, A. F. Molisch, S. Hur, J. Park, and C. J. Zhang, "Spatially consistent street-by-street path loss model for 28-GHz channels in micro cell urban environments," *IEEE Trans. Wireless Commun.*, vol. 16, no. 11, pp. 7538–7550, Nov. 2017.
- [29] S. Ju, O. Kanhere, Y. Xing, and T. S. Rappaport, "A millimeter-wave channel simulator NYUSIM with spatial consistency and human blockage," in *Proc. IEEE Global Commun. Conf. (GLOBECOM)*, Dec. 2019, pp. 1–6.
- [30] X. Cai and G. B. Giannakis, "A two-dimensional channel simulation model for shadowing processes," *IEEE Trans. Veh. Technol.*, vol. 52, no. 6, pp. 1558–1567, Nov. 2003.
- [31] Z. Wang, E. K. Tameh, and A. R. Nix, "Joint shadowing process in urban peer-to-peer radio channels," *IEEE Trans. Veh. Technol.*, vol. 57, no. 1, pp. 52–64, Jan. 2008.
- [32] C. Huang, A. F. Molisch, R. He, R. Wang, P. Tang, and Z. Zhong, "Machine-learning-based data processing techniques for vehicle-to-vehicle channel modeling," *IEEE Commun. Mag.*, vol. 57, no. 11, pp. 109–115, Nov. 2019.
- [33] R. He, B. Ai, A. F. Molisch, G. L. Stuber, Q. Li, Z. Zhong, and J. Yu, "Clustering enabled wireless channel modeling using big data algorithms," *IEEE Commun. Mag.*, vol. 56, no. 5, pp. 177–183, May 2018.
- [34] W. Hu, S. Geng, and X. Zhao, "Mm-wave 60 GHz channel fading effects analysis based on RBF neural network," in *Proc. 5th Int. Conf. Comput. Commun. Syst. (ICCCS)*, Shanghai, China, May 2020, pp. 589–593.
- [35] S. Yiu, M. Dashti, H. Claussen, and F. Perez-Cruz, "Locating user equipments and access points using RSSI fingerprints: A Gaussian process approach," in *Proc. IEEE Int. Conf. Commun. (ICC)*, Kuala Lumpur, Malaysia, May 2016, pp. 1–6.
- [36] Y. Zhang, J. Wen, G. Yang, Z. He, and J. Wang, "Path loss prediction based on machine learning: Principle, method, and data expansion," *Appl. Sci.*, vol. 9, p. 1908, May 2019.
- [37] H.-S. Jo, C. Park, E. Lee, H. K. Choi, and J. Park, "Path loss prediction based on machine learning techniques: Principal component analysis, artificial neural network, and Gaussian process," *Sensors*, vol. 20, no. 7, p. 1927, Mar. 2020.
- [38] J. Thrane, D. Zibar, and H. L. Christiansen, "Model-aided deep learning method for path loss prediction in mobile communication systems at 2.6 GHz," *IEEE Access*, vol. 8, pp. 7925–7936, 2020.

- [39] S. P. Sotirioudis, S. K. Goudos, and K. Siakavara, "Deep learning for radio propagation: Using image-driven regression to estimate path loss in urban areas," *ICT Exp.*, vol. 6, no. 3, pp. 160–165, Sep. 2020.
- [40] R. Adeogun, "Calibration of stochastic radio propagation models using machine learning," *IEEE Antennas Wireless Propag. Lett.*, vol. 18, no. 12, pp. 2538–2542, Sep. 2019.
- [41] N. Moraitis, L. Tsipi, and D. Vouyioukas, "Machine learning-based methods for path loss prediction in urban environment for LTE networks," in *Proc. 16th Int. Conf. Wireless Mobile Comput., Netw. Commun. (WiMob)*, Oct. 2020, pp. 1–6.
- [42] T. S. Rappaport, *Wireless Communications: Principles and Practice*. Upper Saddle River, NJ, USA: Prentice-Hall, 2002, pp. 75–92.
- [43] Y. Sha, X. Xu, and N. Yao, "Wireless channel model based on RBF neural network," in *Proc. 4th Int. Conf. Natural Comput.*, Jinan, China, 2008, pp. 605–609.
- [44] N. Sun, S. Geng, S. Li, X. Zhao, M. Wang, and S. Sun, "Channel modeling by RBF neural networks for 5G mm-wave communication," in *Proc. IEEE/CIC Int. Conf. Commun. China (ICCC)*, Beijing, China, Aug. 2018, pp. 768–772.
- [45] P. Kyösti, "WINNER II channel models part I channel models," Deliverable IST-4-027756 Wireless World Initiative New Radio II (WINNER II) D1.1.2 V.1.2, Eur. Commission, Belgium, 2007.
- [46] V. G. Rossum and F. L. Drake Jr., *Python 3 Reference Manual*. Scotts Valley, CA, USA: CreateSpace, 2009.
- [47] P. Virtanen, R. Gommers, T. E. Oliphant, M. Haberland, T. Reddy, D. Cournapeau, E. Burovski, P. Peterson, W. Weckesser, J. Bright, and S. J. Van Der Walt, "SciPy 1.0: Fundamental algorithms for scientific computing in Python," *Nature Methods*, vol. 17, no. 3, pp. 261–272, Feb. 2020.
- [48] G. G. Alexander de Mattheus, M. Van Der Wilk, T. Nickson, K. Fujii, A. Boukouvalas, P. León-Villagrà, Z. Ghahramani, and J. Hensman, "GPflow: A Gaussian process library using TensorFlow," *J. Mach. Learn. Res.*, vol. 18, no. 40, pp. 1–6, Apr. 2017.
- [49] M. Abadi, J. Chen, Z. Chen, A. Davis, J. Dean, M. Devin, S. Ghemawat, G. Irving, M. Isard, and M. Kudlur, "TensorFlow: A system for large-scale machine learning," in *Proc. 12th USENIX Symp. Operating Syst. Des. Implement. (OSDI)*, Nov. 2016, pp. 265–284.
- [50] D. C. Liu and J. Nocedal, "On the limited memory BFGS method for large scale optimization," *Math. Program.*, vol. 45, no. 1, pp. 503–528, 1989.
- [51] G. E. Fasshauer, *Meshfree Approximation Methods With MATLAB*. Singapore: World Scientific, 2007.
- [52] C. E. Rasmussen and C. K. I. Williams, *Gaussian Processes for Machine Learning*. Cambridge, MA, USA: MIT Press, 2006.



JUNSEOK KIM (Member, IEEE) received the B.S. and M.S. degrees in electrical engineering from the Pohang University of Science and Technology (POSTECH), Pohang, South Korea, in 2017 and 2019, respectively. Since 2019, he has been with the Electronics and Telecommunications Research Institute (ETRI), Daejeon, South Korea. His research interests include radio propagation, wireless channel measurement and modeling, and 5G physical layer specifications.



YOUNGKEUN YOON received the B.E. and M.E. degrees in radio engineering from Chungbuk National University, Cheongju, South Korea, in 1997 and 1999, respectively. Since 2000, he has been worked at the Electronics and Telecommunications Research Institute (ETRI). He has been involved in the research of simulation and evaluation for the Radio Resource Management based on the multiple CDMA systems, since 2003. He was a Visiting Researcher at the Center for Communication Systems Research (CCSR), University of Surrey, U.K., from 2003 to 2004. He has been involved in the analysis of the impacts for interference between existing system and new system. His research interests include system performance and evaluations, radio propagation, and artificial intelligence based on radio communication systems.



CHUNG-SUP KIM received the B.S. and M.S. degrees in electrical engineering from Kyungpook National University, Daegu, South Korea, in 1997 and 1999, respectively. Since 1999, he has been with the Electronics and Telecommunications Research Institute as a Principal Researcher. His research interests include direction finding, beamforming, RADAR, radio propagation, and 5G communication.

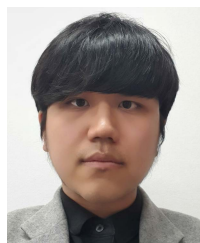


YOUNG-JUN CHONG received the B.S. degree from Jeju University, Jeju, South Korea, in 1992, the M.S. degree in electronics engineering from the Sogang University, Seoul, South Korea, in 1994, and the Ph.D. degree in electronic engineering from the Chungnam National University, Daejeon, South Korea, in 2005. Since 1994, he has been with the Electronics and Telecommunications Research Institute, where he is a Principle Member of the Research Staff at the Radio Resource Research Section. He served as a Project Leader involved in the research for spectrum engineering. His research interests include RF circuit and systems, radio interference, mobile communications, and interference modeling. He is a member of KIEES.



GANGUK HWANG (Member, IEEE) received the B.S., M.S., and Ph.D. degrees in mathematics (applied probability) from the Korea Advanced Institute of Science and Technology (KAIST), Daejeon, South Korea, in 1991, 1993, and 1997, respectively. From February 1997 to March 2000, he was with the Electronics and Telecommunications Research Institute (ETRI), Daejeon. From March 2000 to February 2002, he was a Visiting Scholar with the School of Interdisciplinary Computing and Engineering, University of Missouri-Kansas City. From August 2010 to July 2011, he was a Visiting Scholar with the Department of Electrical Engineering, University of Washington, Seattle, WA, USA. Since March 2002, he has been with the Department of Mathematical Sciences, KAIST, where he is currently a Professor. His research interests include performance modeling and optimization of wired/wireless networks, machine learning with Gaussian processes, Bayesian inference, and deep learning.

...



KI JOUN JANG received the B.S. degree in mathematical science and computer science from the Korea Advanced Institute of Science and Technology (KAIST), Daejeon, South Korea, in 2018, where he is currently pursuing the Ph.D. degree with the Department of Mathematical Sciences. His research interests include machine learning, Gaussian processes, deep learning, and image synthesis and pattern recognition.



SEJUN PARK received the B.S. degree in mathematics education from Seoul National University (SNU), Seoul, South Korea, in 2019. He is currently pursuing the Ph.D. degree with the Department of Mathematical Sciences, Korea Advanced Institute of Science and Technology (KAIST), Daejeon, South Korea. His research interests include machine learning with Gaussian processes, federated learning, and reinforcement learning.